PERGAMON

International Journal of Multiphase Flow 25 (1999) 1073–1097

International Journal of Multiphase Flow

www.elsevier.com/locate/ijmulflow

Modeling high-speed viscous liquid sheet atomization

P.K. Senecal, D.P. Schmidt, I. Nouar, C.J. Rutland, R.D. Reitz, M.L. Corradini*

Engine Research Center, University of Wisconsin-Madison, Madison, WI 53706, USA

Received 22 March 1999; received in revised form 18 May 1999

Professor Hetsroni: It is an honor to be part of your Festschrift celebration. We have read your past work with great interest, and we expect that your important efforts will continue far into the future.

Abstract

A linear stability analysis is presented for a liquid sheet that includes the effects of the surrounding gas, surface tension and the liquid viscosity on the wave growth process. An inviscid dispersion relation is used to identify the transition from a long wavelength regime to a short wavelength regime, analogous to the first and second wind induced breakup regimes of cylindrical liquid jets. This transition, which is found to occur at a gas Weber number of 27/16, is used to simplify the viscous dispersion relation for use in multi-dimensional simulations of sheet breakup. The resulting dispersion relation is used to predict the maximum unstable growth rate and wave length, the sheet breakup length and the resulting drop size for pressure-swirl atomizers. The predicted drop size is used as a boundary condition in a multi-dimensional spray model. The results show that the model is able to accurately predict liquid spray penetration, local Sauter mean diameter and overall spray shape.

Keywords: Sheet atomization; Hydrodynamic instability; Drop distortion; Breakup; Multi-dimensional modeling

1. Introduction

Pressure-swirl atomizers are widely used in gas turbine engines, industrial furnaces, agricultural sprays, and gasoline direct injection automotive engines. These atomizers generate a thin, liquid sheet which spreads radially due to the initial swirl. The purpose of the atomizers

* Corresponding author. Tel.: +1-608-265-2001; fax: +1-608-262-6400.
E-mail address: corradini@engr.wisc.edu (M.L. Corradini)

0301-9322/99/$ - see front matter
PII: S0301-9322(99)00057-9

is to produce small drops spread over a wide angle. In order to model the drop formation process, one must postulate a mechanism of sheet breakup and pose a mathematical formulation of this mechanism. Past researchers, such as Taylor (1940), Dombrowski and Johns (1963), and others have speculated that the drop sizes may be correlated with the wavelengths that grow on the surface of the sheet. Dombrowski and Johns derived a dispersion relation for the growth rate of long waves with infinitesimal amplitude, including the effects of surface tension, aerodynamic forces, and liquid viscosity. They identified the wavelength with the largest growth rate and assumed that this wave broke up the sheet at half wavelength intervals into ligaments. The ligaments then broke up into droplets, according to Weber's theory for a cylindrical liquid column. This methodology, shown in Fig. 1, has been widely used, as in the case of Mitra and Li (1998). It should be noted that other sheet breakup mechanisms have also been observed. For example, Stapper et al. (1992) identified a 'stretched stream-wise ligament breakup' regime which occurs at low liquid velocities with coflowing air. In this regime, stream-wise vortical waves become amplified and thin liquid membranes are formed in between them. Eventually the membranes burst, forming small drops, while the vortical waves produce stream-wise ligaments which breakup into relatively large drops (Stapper et al., 1992). A second regime, or 'cellular breakup' regime, was found to occur at higher relative velocities. In this regime, both stream-wise and span-wise waves are present (Stapper et al., 1992). The stream-wise waves and connecting membranes burst to form small droplets, while the span-wise waves detach to form ligaments as in Fig. 1. These ligaments undergo further breakup to form droplets. The present study is restricted to the growth of span-wise waves as suggested by Dombrowski and Johns (1963).

Though Dombrowski and John's breakup mechanism is supported experimentally, as in Crapper et al. (1973), there are some unresolved issues with their mathematical assumptions. First, Dombrowski and Johns used a one-dimensional model of the liquid film by neglecting any variation in the y-direction within the sheet (see Fig. 2 for the coordinate axes). As will be shown in a following section, such an assumption, which was also made by Weihs (1978), cannot be used for a viscous sheet. Thus, the assumptions of Dombrowski and Johns lead to a contradiction and an inaccurate dispersion equation. Furthermore, Dombrowski and Johns, like Squire (1953), assumed long waves. However, under the conditions found in modern

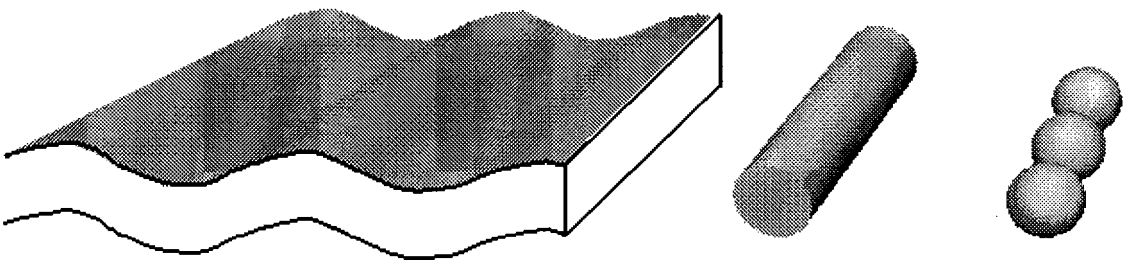

Fig. 1. Schematic of the sheet disintegration and drop formation processes as proposed by Dombrowski and Johns (1963).

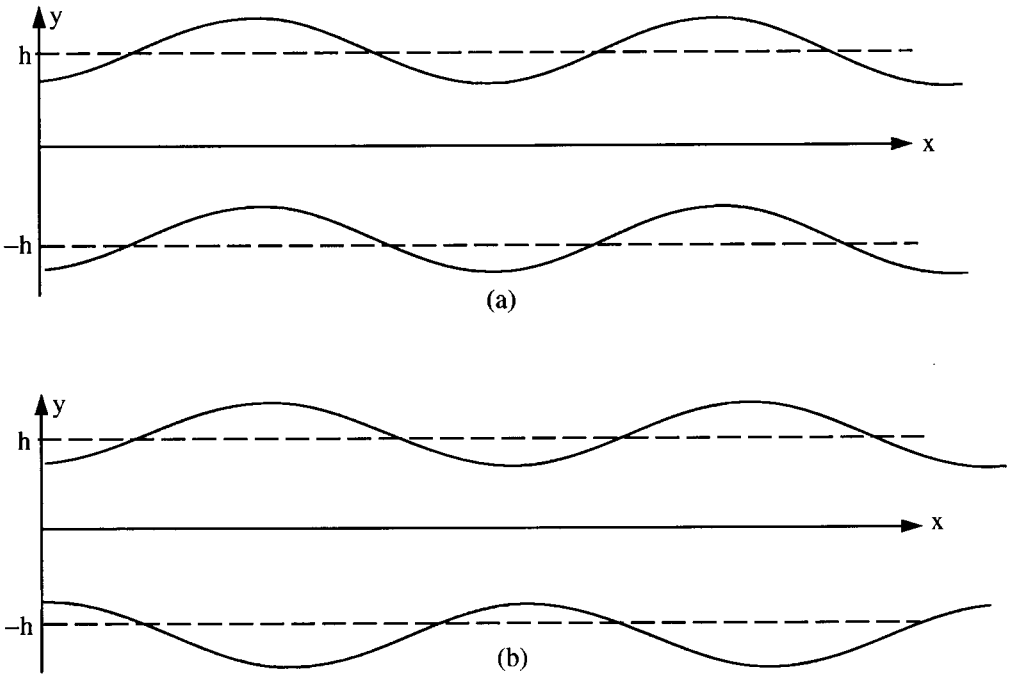

Fig. 2. Schematic of (a) antisymmetric or sinuous waves and (b) symmetric or varicose waves.

atomizers, the long wave assumption leads to inaccuracies in the predicted sheet stability. Li and Tankin (1991) and Hagerty and Shea (1955) did not make this assumption, but only Li and Tankin included the effects of viscosity. Hagerty and Shea also assumed that the ratio of gas-to-liquid density was much smaller than the hyperbolic tangent of the product of wave number and sheet thickness (for sinuous waves). The present work indicates that this assumption leads to inaccuracies at very low gas Weber numbers. On the other hand, Li and Tankin's viscous result is quite general, but it is also somewhat cumbersome for use in multi-dimensional models, requiring the numerical solution of a non-linear, complex equation.

While extensive research has been performed in an attempt to understand the linear and non-linear behavior of liquid sheets, the current state-of-the-art in hollow-cone spray modeling either ignores the primary atomization process (e.g., Xu and Markle, 1998; VanDerWege, 1999), or utilizes results based on inviscid theory simplified by long wave assumptions (e.g., Han et al., 1997; Ren and Nally, 1998). On the other hand, the goal of the present work is the formulation of a sheet breakup model including the effects of liquid viscosity, surface tension and the surrounding gas which can be readily implemented in multi-dimensional simulations of transient sprays. An analysis for the growth of sinuous waves on a thin liquid sheet surrounded by a stationary gas is presented and shown to be consistent with Li and Tankin's (Li and Tankin, 1991) general, viscous dispersion relation. The inviscid expressions of Hagerty and Shea (1955) and Squire (1953) are also recovered when the same assumptions are applied to the present expression. Using an inviscid model equation, a critical Weber number for the transition from long to short wave growth is derived. It is shown that the long wave regime is

dominant for low-speed sheet atomization, while short waves are responsible for breakup in the case of high-speed sheets, primarily of interest in the present work. This result is used to simplify the general viscous expression and derive new dispersion relations in each regime for application to thinning viscous sheets. A long wave expression is presented which corrects the coefficients of the viscous terms in Dombrowski and John's (Dombrowski and Johns, 1963) dispersion relation. In addition, the maximum growth rates and corresponding wave numbers as predicted from the short wave expression are shown to agree well with numerical solutions of the general dispersion relation. When combined with current secondary breakup, drop drag and collision models, the present primary atomization model is shown to accurately predict experimentally measured spray features for both inwardly and outwardly opening pressure-swirl atomizers.

2. Linear stability analysis

The present stability analysis for a liquid sheet, which includes the effects of the surrounding gas and liquid viscosity, is formulated from the equations of motion and follows the approach of Sterling and Sleicher (1975), Levich (1962) and Reitz and Bracco (1986) for the analysis of the stability of cylindrical liquid jets.

Consider a two-dimensional, viscous, incompressible liquid sheet of thickness $2h$ moving with velocity U through a quiescent, inviscid, incompressible gas medium. The liquid and gas have densities of ρ_1 and ρ_2, respectively, and the viscosity of the liquid is μ_1.[1] A coordinate system is used which moves with the sheet, and a spectrum of infinitesimal disturbances of the form

$$\eta = \Re\left[\eta_0 \exp(ikx + \omega t)\right] \tag{1}$$

are imposed on the initially steady motion. The instability produces fluctuating velocities and pressures u_1, v_1 and p_1 for the liquid, and u_2, v_2 and p_2 for the gas. In Eq. (1), η_0 is the initial wave amplitude, $k = 2\pi/\lambda$ is the wave number, and $\omega = \omega_r + i\omega_i$ is the complex growth rate. The most unstable disturbance has the largest value of ω_r, denoted by Ω_s in the present work, and is assumed to be responsible for breakup. The resulting ligament size is related to the maximum unstable wavelength $\Lambda_s = 2\pi/K_s$ where K_s is the wave number corresponding to the maximum growth rate Ω_s. Thus, it is desired to obtain a dispersion relation $\omega = \omega(k)$ from which the most unstable disturbance can be deduced.

To obtain the dispersion relation, the linearized liquid continuity and momentum equations must be solved subject to the following linearized boundary conditions at the interfaces ($y = \pm h$) between the liquid and gas:

$$v_1 = \frac{\partial \eta}{\partial t} \tag{2}$$

[1] In the present work, subscript 1 refers to quantities for the liquid phase, and subscript 2 refers to quantities for the gas phase.

$$\frac{\partial v_1}{\partial x} = -\frac{\partial u_1}{\partial y} \tag{3}$$

$$-p_1 + 2\mu_1 \frac{\partial v_1}{\partial y} + p_2 = \sigma \frac{\partial^2 \eta}{\partial x^2} \tag{4}$$

where σ is the surface tension. Eqs. (2)–(4) are mathematical statements of the kinematic free surface condition, continuity of shear stress (or zero shear stress at the surface since the gas is assumed inviscid) and continuity of normal stress, respectively.

The linearized equations of motion for the gas must also be solved in order to obtain the gas pressure, p_2, in Eq. (4). The gas phase boundary conditions require that

$$v_2 = \frac{\partial \eta}{\partial t} + U \frac{\partial \eta}{\partial x} \tag{5}$$

at the interfaces ($y = \pm h$) and that

$$u_2, v_2, p_2 \rightarrow 0 \tag{6}$$

far from the interface ($y \rightarrow \infty$).

In order to solve the liquid equations, the velocities are separated into two parts using the Helmholtz decomposition:

$$u_1 = u_\mathrm{I} + u_\mathrm{R} = \frac{\partial \phi_1}{\partial x} - \frac{\partial \psi_1}{\partial y} \tag{7}$$

$$v_1 = v_\mathrm{I} + v_\mathrm{R} = \frac{\partial \phi_1}{\partial y} + \frac{\partial \psi_1}{\partial x} \tag{8}$$

where u_I and v_I are the irrotational solutions, and u_R and v_R contain the effects of viscosity. With the velocity potential

$$\phi_1 = \varphi(y)\exp(ikx + \omega t) \tag{9}$$

and stream function

$$\psi_1 = \chi(y)\exp(ikx + \omega t) \tag{10}$$

defined in Eqs. (7) and (8), the liquid equations give

$$p_1 = -\rho_1 \frac{\partial \phi_1}{\partial t}, \tag{11}$$

$$\varphi_1''(y) - k^2 \varphi_1(y) = 0 \tag{12}$$

and

$$\chi_1''(y) - \mathscr{L}^2 \chi_1(y) = 0 \tag{13}$$

where $\mathscr{L}^2 = k^2 + \omega/\nu_1$ and the primes denote differentiation with respect to y. Solutions to Eqs. (12) and (13), subject to the boundary conditions, give ϕ_1 and ψ_1 and hence u_1 and v_1 for the liquid. Furthermore, once the velocity potential is known, Eq. (11) gives the liquid pressure.

As determined by Squire (1953) and Hagerty and Shea (1955) for the case of inviscid sheets, two solutions, or modes, exist which satisfy Eqs. (12) and (13) subject to the boundary conditions at the upper and lower interfaces. For the first solution, called the sinuous mode, the waves at the upper and lower interfaces are exactly in phase as shown in Fig. 2(a). On the other hand, for the varicose mode, the waves are π radians out of phase as shown in Fig. 2(b). For the case of sinuous waves, solutions for the liquid velocity potential and stream function are given by

$$\phi_1 = C_1 \frac{\cosh(\mathscr{L}h)}{\cosh(kh)} \frac{\left(\mathscr{L}^2 + k^2\right)}{2ik^2} \sinh(ky)\exp(ikx + \omega t) \tag{14}$$

and

$$\psi_1 = C_1 \cosh(\mathscr{L}y)\exp(ikx + \omega t), \tag{15}$$

respectively, where C_1 is a constant of integration.

If a stream function is also defined for the gas phase and is assumed to have the form

$$\psi_2 = (U - c)\eta f(y) \tag{16}$$

where $c = i\omega/k$ is the phase velocity, it can be shown that the gas equations give the following differential equation for f:

$$f'' + \frac{2U'}{U - c} f' - k^2 f = 0 \tag{17}$$

where primes denote differentiation with respect to y. If the boundary conditions given by Eqs. (5) and (6) are mapped into f-space and it is assumed that $U(y)$ is constant (i.e., slip at the interface), Eq. (17) can be solved to give

$$f = \exp\left[k(h - y)\right]. \tag{18}$$

Furthermore, the gas pressure is given by

$$p_2 = \rho_2 \eta (U - c)^2 f'. \tag{19}$$

When the velocity and pressure solutions are substituted into the normal stress condition, Eq. (4), the following dispersion relation between ω and k is obtained for the case of sinuous waves:

$$\omega^2\left[\tanh(kh) + Q\right] + \omega\left[4\nu_1 k^2 \tanh(kh) + 2iQkU\right] + 4\nu_1^2 k^4 \tanh(kh)$$

$$-4\nu_1^2 k^3 \mathscr{L} \tanh(\mathscr{L}h) - QU^2 k^2 + \frac{\sigma k^3}{\rho_1} = 0 \tag{20}$$

where $Q = \rho_2/\rho_1$. Note that a similar analysis gives the dispersion relation for the varicose mode, which can also be obtained by replacing $\tanh(kh)$ and $\tanh(\mathscr{L}h)$ in Eq. (20) with $\coth(kh)$ and $\coth(\mathscr{L}h)$, respectively.

Li and Tankin (1991) derived a dispersion relation similar to Eq. (20) for a viscous sheet in the sinuous mode. Their equation, which was obtained from a linear analysis with a stationary coordinate system, can also be used to obtain Eq. (20). This is accomplished by replacing ω by $\omega - ikU$ and by also noting that U has opposite sign in the stationary coordinate system. A viscous dispersion relation has also been derived by Lin et al. (1990) who examined the absolute and convective instability of liquid sheets subject to disturbances growing both spatially and temporally.

3. Solutions of the dispersion relation

3.1. Inviscid sheets

While the viscous solution will be used to predict the sheet breakup length and subsequent drop sizes in a following section, the simpler inviscid solutions can be used to provide guidelines in formulating the appropriate assumptions to simplify Eq. (20). Thus, if viscosity is neglected, Eq. (20) reduces to

$$\omega^2\big[\tanh(kh) + Q\big] + \omega 2iQkU - QU^2k^2 + \frac{\sigma k^3}{\rho_1} = 0 \tag{21}$$

for the sinuous mode and

$$\omega^2\big[\coth(kh) + Q\big] + \omega 2iQkU - QU^2k^2 + \frac{\sigma k^3}{\rho_1} = 0 \tag{22}$$

for the varicose mode. Solutions to Eqs. (21) and (22) for the growth rate ω_r are given by

$$\omega_r = \frac{\sqrt{\tanh(kh)QU^2k^2 - \sigma k^3/\rho_1\big[\tanh(kh) + Q\big]}}{\tanh(kh) + Q} \tag{23}$$

and

$$\omega_r = \frac{\sqrt{\coth(kh)QU^2k^2 - \sigma k^3/\rho_1\big[\coth(kh) + Q\big]}}{\coth(kh) + Q}, \tag{24}$$

respectively. Note that Eqs. (23) and (24) reduce to the growth rate expressions of Hagerty and Shea (1955) if it is assumed that $Q \ll \tanh(kh)$.

Eqs. (23) and (24) for the sinuous and varicose growth rates are shown in Figs. 3 and 4 for gas Weber numbers $We_2 = \rho_2U^2h/\sigma$ of 0.5 and 5.0, respectively. It is clear that for the low Weber number case, the growth of sinuous waves dominate the growth of varicose waves due to the higher growth rates throughout the range of instability. On the other hand, for a We_2

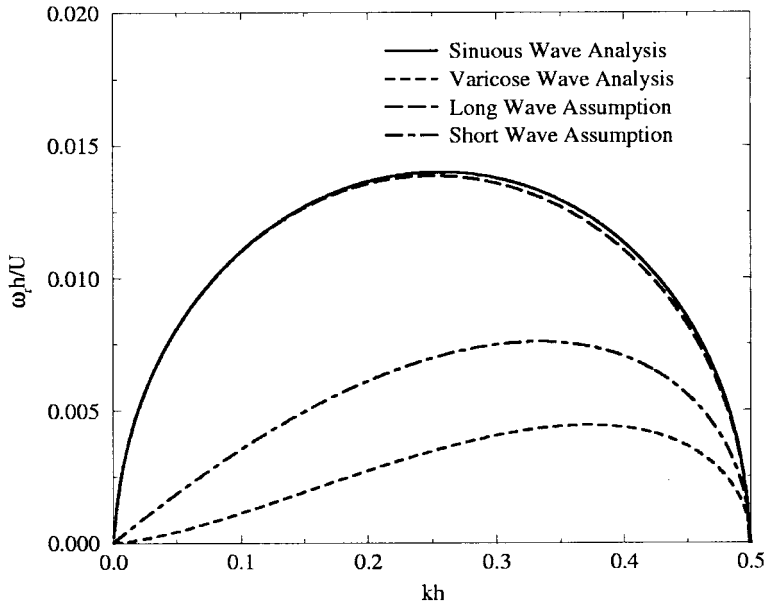

Fig. 3. Inviscid dimensionless growth rates $\omega_r h/U$ as functions of dimensionless wave number kh for a gas Weber number of $We_2 = 0.5$.

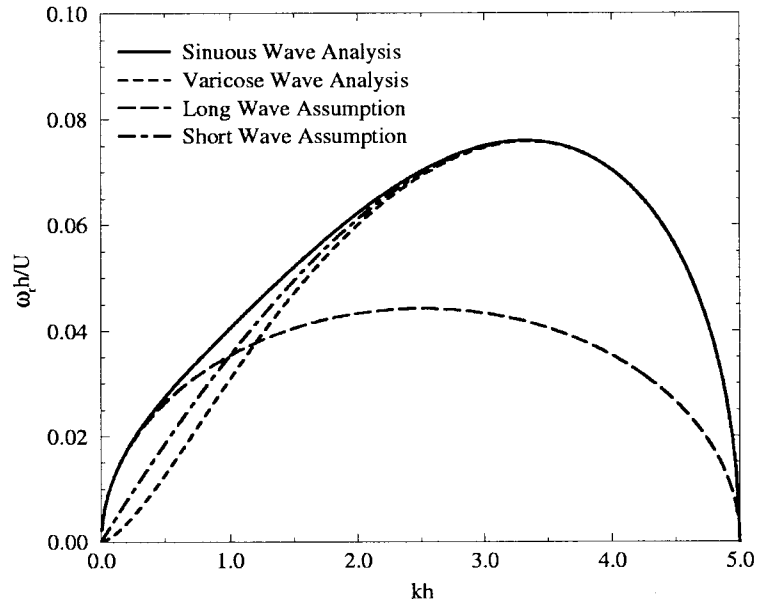

Fig. 4. Inviscid dimensionless growth rates $\omega_r h/U$ as functions of dimensionless wave number kh for a gas Weber number of $We_2 = 5.0$.

value of 5.0, the dimensionless growth rate curves are very similar, except at low values of the dimensionless wave number kh, suggesting that the two modes are indistinguishable or that the wave growth on one interface is independent of the growth on the other.

The above results suggest that the maximum growth rate of sinuous waves will always be greater or equal to the maximum growth rate of varicose waves for the conditions of interest in the present study. This was also deduced by Hagerty and Shea (1955) and Squire (1953), who assumed that long waves grow on the interfaces so that $\tanh(kh) \approx kh$. Eqs. (23) and (24) also indicate that the varicose mode is more unstable for density ratios near unity, as also determined by Rangel and Sirignano (1991). However, in the present work Q is significantly less than one and thus it is assumed that sinuous wave growth dominates.

With the long wave assumption described above, Eq. (23) reduces to

$$\omega_r = \frac{\sqrt{QU^2k^3h - \sigma k^3/\rho_1(kh + Q)}}{kh + Q} \tag{25}$$

which is identical to Squire's result if it is further assumed that $Q \ll kh$ so that[2]

$$\omega_r = \sqrt{\frac{QU^2k^2 - \sigma k^3/\rho_1}{kh}}. \tag{26}$$

A comparison of Eq. (26) with the sinuous mode solution is given in Figs. 3 and 4 for gas Weber numbers of 0.5 and 5.0, respectively. As shown in the figures, the long wave assumption agrees very well for the low Weber number case, however, for the higher Weber number case Eq. (26) is a poor approximation of the general inviscid sinuous mode growth rate expression, Eq. (23). While long waves have been seen to grow on the surfaces of low velocity sheets experimentally, it is possible that short waves grow at higher velocities or higher Weber numbers. In fact, the range of instability, and in particular, the dominant unstable dimensionless wave number in Fig. 4 suggests that this is indeed the case. Thus, if short waves are assumed, $\tanh(kh) = \coth(kh) = 1$ and both Eqs. (23) and (24) reduce to

$$\omega_r = \frac{\sqrt{QU^2k^2 - \sigma k^3/\rho_1(1 + Q)}}{1 + Q} \tag{27}$$

which can be further simplified to

$$\omega_r = \sqrt{QU^2k^2 - \sigma k^3/\rho_1} \tag{28}$$

in the limit of $Q \ll 1$.

A comparison of Eqs. (26) and (28) indicates that $\omega_{r,short} = \sqrt{kh}\omega_{r,long}$. In other words, short wave growth will dominate long wave growth only if $kh > 1$ or equivalently if $\lambda/h < 2\pi$. This is clear from Fig. 4 for $We_2 = 5.0$, which includes a plot of Eq. (28). However, for a We_2 of 0.5

[2] In the present study, the liquid considered is automotive fuel which is injected into air at atmospheric conditions. Q is of the order of 10^{-3} and this assumption is reasonable for typical injection conditions.

(see Fig. 3), $kh<1$ for the range of instability and thus long waves dominate over the entire spectrum of wave numbers.

The present results indicate that the long wave assumption is in good agreement with the general sinuous analysis for a We_2 of 0.5, while the short wave assumption predicts the maximum growth rate of the general analyses very well for a We_2 of 5.0. The fact that the long wave analysis predicts lower Weber number growth while the short wave analysis predicts higher Weber number growth indicates that there is a cutoff, or critical Weber number, below which long waves dominate and above which short waves dominate. This is shown in Fig. 5 which gives the dimensionless breakup length L/h (see Eq. (35)), as a function of We_2 for the general sinuous, short wave and long wave analyses. As indicated in the figure, the critical We_2 can be determined as the point where the breakup lengths (or maximum growth rates) for the long and short wave analyses are equal. For We_2 below this value the long wave approximation accurately predicts the breakup length, while the short wave approximation is in very good agreement with the general sinuous analysis for We_2 above this value. Thus, if the dimensionless maximum growth rate for the long wave analysis (Eq. (26)) given by

$$\left[\frac{\Omega_s h}{U}\right]_{\text{long}} = \frac{1}{2}\sqrt{QWe_2}, \tag{29}$$

which occurs at a dimensionless wave number of $K_s h = 1/2We_2$, is equated with the dimensionless maximum growth rate for the short wave analysis (Eq. (28)) given by

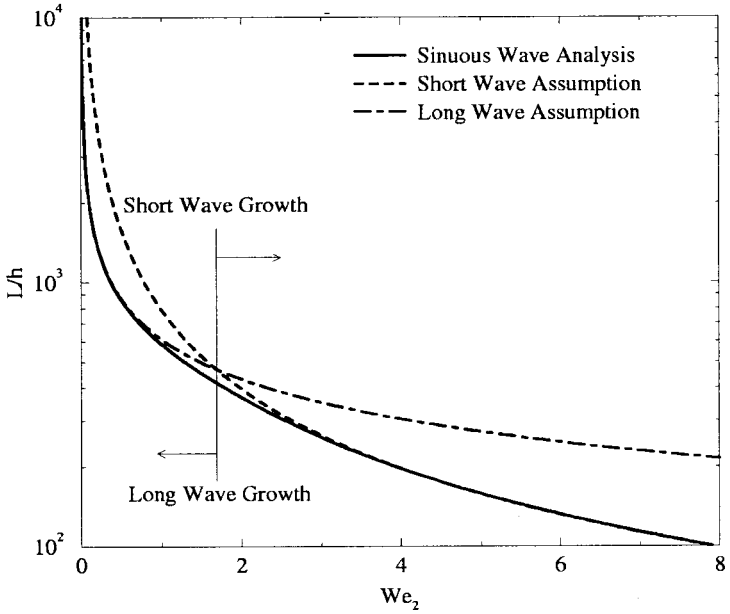

Fig. 5. Dimensionless breakup length as a function of We_2 for the general, inviscid sinuous, long wave and short wave analyses.

$$\left[\frac{\Omega_s h}{U}\right]_{\text{short}} = \frac{2}{3} We_2 \sqrt{\frac{Q}{3}}, \tag{30}$$

which occurs at $K_s h = 2/3 We_2$, it can be shown that the critical Weber number (based on the sheet half thickness h) is given by $We_2 = 27/16$.

While Eq. (26) for long waves was shown to be valid for moderate We_2 below the critical value of 27/16 (see Fig. 3), the assumption that $Q \ll kh$ breaks down for very low gas Weber numbers. This is illustrated in Fig. 6 which gives the dimensionless growth rates obtained from Eqs. (25) and (26) as functions of the dimensionless wave number for a We_2 of 0.05. It is clear from this figure that Eq. (26) overpredicts both the maximum growth rate and the range of instability. It can be shown that Eq. (25) predicts that unstable waves will grow for $kh < We_2 - Q$ while the instability range for Eq. (26) is given by $kh < We_2$. As a result, Eq. (26) should be used with caution for very low We_2. This may be the case for very low film velocities and/or very thin sheets.

The identification of long and short wavelength regimes for liquid sheet breakup is similar to the first and second wind induced regimes for cylindrical jet breakup (Reitz and Bracco, 1986). However, while the gas inertia assists the surface tension force in the destabilization process for jets (in the first wind induced regime), surface tension is stabilizing for sheets. This is apparent if Q is set to zero in either Eq. (26) or (28) so that only surface tension is acting on the sheet. Thus, for a sheet the breakup length decreases continuously as the gas Weber number is increased (see Fig. 5) while the destabilizing effect of surface tension on a jet causes the breakup length to grow from zero to a maximum and then decrease again as We_2 is increased (Reitz and Bracco, 1986).

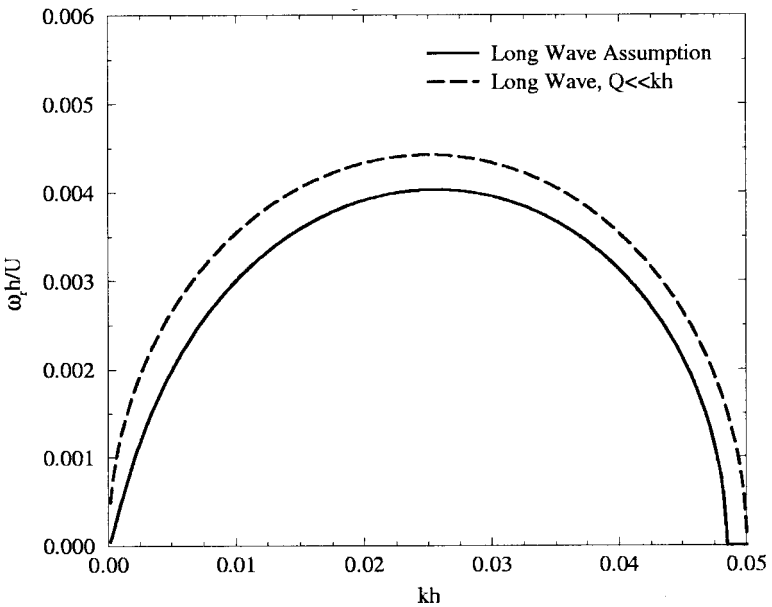

Fig. 6. Inviscid dimensionless growth rates $\omega_r h/U$ as functions of dimensionless wave number kh for a gas Weber number of $We_2 = 0.05$.

Levich (1962) analyzed the inviscid dispersion relation for a cylindrical jet in the limit of $ka \gg 1$, where a is the jet radius. With this assumption it was found that the dispersion relation reduced to Eq. (28), which suggests that short waves are independent of the nature of the surface on which they grow. Note, however, that short waves begin to dominate for sheets if $\lambda/h<2\pi$, i.e., if the wavelength is less than about six times the sheet half thickness. Thus, the wavelengths of these short waves are not necessarily smaller than the thickness of the sheet. On the other hand, Eq. (28) was derived for jets only in the limit that the jet radius is much larger than the wavelength, in which case the curvature of the surface has no effect on the instability.

3.2. Viscous sheets

As stated above, Li and Tankin (1991) derived a dispersion relation similar to Eq. (20) for a viscous sheet from a linear analysis with a stationary coordinate system. The full equation was solved numerically to obtain ω_r as a function of k for various conditions, and to examine the effects of liquid viscosity on the instability. While Li and Tankin's dispersion relation is quite general, a simplified relation which captures the essential features of Eq. (20) would be beneficial for application to multi-dimensional simulations. Thus, the results of Section 3.1 for an inviscid liquid are used in this section to produce a closed-form expression for viscous sheets.

Dombrowski and Johns (1963) provided a simplified dispersion relation from an analysis of the aerodynamic instability and disintegration of viscous sheets and obtained a growth rate expression for long waves. However the effect of viscosity is underpredicted in their result due to the assumptions in the formulation. In particular, Dombrowski and Johns treated the film as one-dimensional by assuming no variation in the y-direction (see Fig. 2). As a result, the shear stress is given by $\tau_{yx} = \mu_1(\partial v/\partial x)$ throughout the sheet, including the boundaries. However, this is inconsistent with the necessary condition of continuity of shear stress at the interfaces. The assumption of an inviscid gas would then imply that τ_{yx} is zero at the interface. Thus, while the analysis of Dombrowski and Johns reduces to the correct dispersion relation for an inviscid liquid with long wave growth, their approach is inconsistent when the effect of viscosity is included.

To provide a simplified viscous dispersion relation, Eq. (20) for sinuous waves is further analyzed. First of all, an order of magnitude analysis using typical values of K_s and Ω_s from the inviscid solutions shows that the terms of second order in viscosity can be neglected in comparison to the other terms in Eq. (20). Thus, with this simplification, the growth rate for the sinuous mode is given by

$$\omega_r = -\frac{2\nu_1 k^2 \tanh(kh)}{\tanh(kh)+Q} + \frac{\sqrt{4\nu_1^2 k^4 \tanh^2(kh) - Q^2 U^2 k^2 - \left[\tanh(kh)+Q\right]\left(-QU^2k^2 + \sigma k^3/\rho_1\right)}}{\tanh(kh)+Q} \tag{31}$$

For long waves in the limit of $Q \ll kh$, Eq. (31) reduces to

$$\omega_r = -2\nu_1 k^2 + \sqrt{4\nu_1^2 k^4 + \frac{QU^2 k}{h} - \frac{\sigma k^2}{\rho_1 h}} \tag{32}$$

which is similar to Dombrowski and John's expression, but with the correct coefficients for the viscous terms (Dombrowski and John's expression can be obtained by dividing each of the viscous terms in Eq. (32) by four). Furthermore, if short waves are assumed for high-speed sheets and $Q \ll 1$, Eq. (31) reduces to

$$\omega_r = -2\nu_1 k^2 + \sqrt{4\nu_1^2 k^4 + QU^2 k^2 - \frac{\sigma k^3}{\rho_1}} \tag{33}$$

which would also be obtained from the dispersion relation for the varicose mode for the same assumptions. Eqs. (32) and (33) are presented in Figs. 7 and 8 with their inviscid counterparts for a We_2 of 0.5 and 5.0, respectively. It is clear from these figures that the inclusion of viscosity reduces both the maximum growth rate and the corresponding wave number, as in the case of liquid jets, without altering the instability range of $kh<We_2$. In addition, the effect of viscosity is minimal for Squire's regime (i.e., for $We_2<27/16$ or long wave growth), as shown in Fig. 7, while the inclusion of the viscous terms are necessary to accurately predict the wave growth of short waves as shown in Fig. 8.

In order to validate the assumptions used to reduce Eq. (20) to Eq. (33) for high Weber numbers, numerical solutions of the maximum growth rate and corresponding wavenumber were calculated via Muller's method. Table 1 presents the dimensionless growth rates and wavenumbers for gas-phase Weber numbers of 5.0 and 10.0 for Eqs. (20), (31) and (33). It is

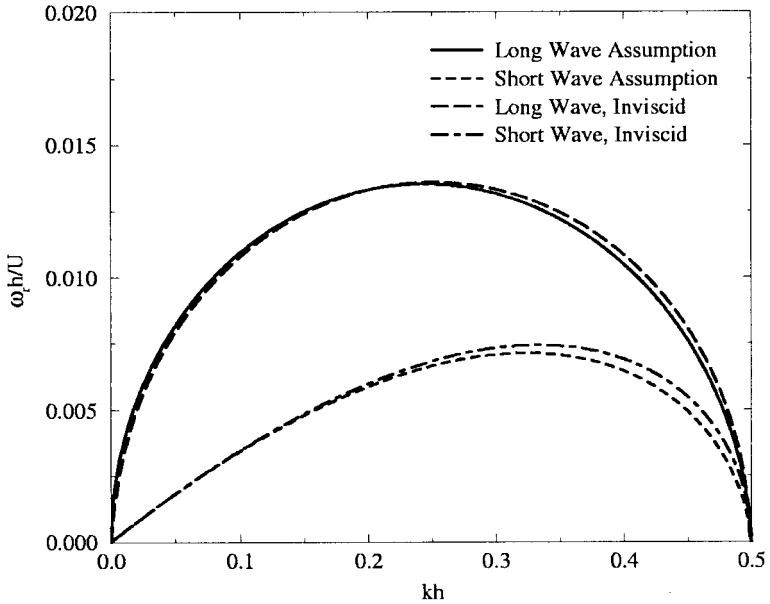

Fig. 7. Viscous and inviscid dimensionless growth rates $\omega_r h/U$ as functions of dimensionless wave number kh for a gas Weber number of $We_2 = 0.5$.

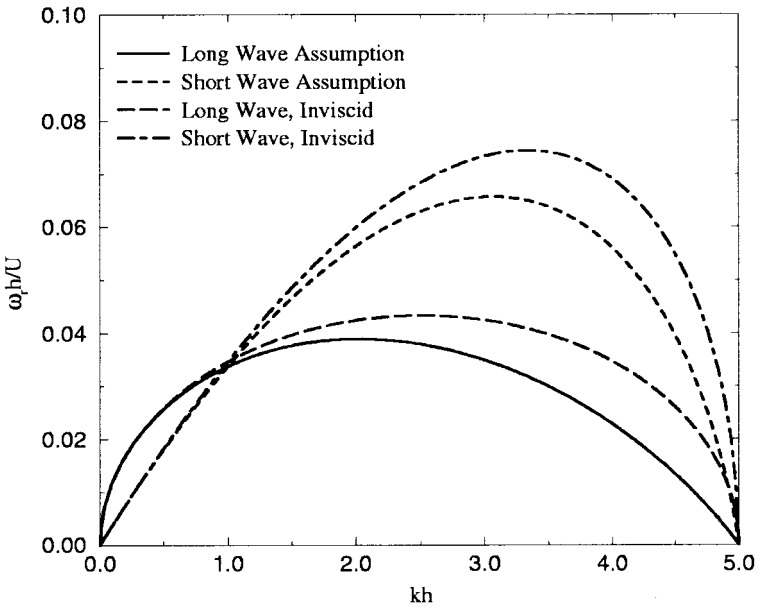

Fig. 8. Viscous and inviscid dimensionless growth rates $\omega_r h/U$ as functions of dimensionless wave number kh for a gas Weber number of $We_2 = 5.0$.

clear from the calculations that the present simplified dispersion relation adequately captures the wave growth process for high-speed sheets.

4. Methodology for modeling sheet breakup and drop formation

4.1. Breakup mechanism

In the present work, the physical mechanism of sheet disintegration proposed by Dombrowski and Johns (1963) is adopted in order to predict the drop sizes produced from the primary breakup process. As shown in Fig. 1, disintegration occurs due to the growth of waves

Table 1
Comparison of dimensionless maximum growth rates $\Omega_s h/U$ and wavenumbers $K_s h$ for the general, viscous dispersion relation Eq. (20), Eq. (31) and the simplified short wave expression Eq. (33)

	Eq. (20)	Eq. (31)	Eq. (33)
$We_2 = 5.0$			
$\Omega_s h/U$	0.0660	0.0633	0.0633
$K_s h$	3.0623	2.9051	2.9323
$We_2 = 10.0$			
$\Omega_s h/U$	0.1180	0.1082	0.1085
$K_s h$	5.7239	5.2841	5.2918

on the surfaces caused by the aerodynamic forces acting on the sheet. Once the waves reach a critical amplitude, fragments of liquid are broken off which contract to form cylindrical ligaments that are believed to move normal to the ligament axis. As a result, capillary forces cause the unstable ligaments to break into drops.

Eqs. (32) and (33) indicate that while the growth rate of long waves depends on the sheet thickness, the growth rate of short waves is independent of the thickness of the sheet. Thus, in order to predict the onset of ligament formation for short wave growth ($We_2 > 27/16$), a sheet breakup length is formulated based on the analogy of the prediction of the breakup length of cylindrical liquid jets (e.g., Reitz and Bracco, 1986). If the surface disturbance has reached a value of η_b at breakup, a breakup time τ can be evaluated via:

$$\eta_b = \eta_0 \exp(\Omega_s \tau) \Longrightarrow \tau = \frac{1}{\Omega_s} \ln\left(\frac{\eta_b}{\eta_0}\right) \tag{34}$$

where Ω_s is the maximum growth rate obtained from Eq. (33). Thus, the sheet will break up at a length given by

$$L = V\tau = \frac{V}{\Omega_s} \ln\left(\frac{\eta_b}{\eta_0}\right) \tag{35}$$

where the quantity $\ln(\eta_b/\eta_0)$ is given the value 12 in the present study based on the work of Dombrowski and Hooper (1962). It is important to note that the quantity V in Eq. (35) is the absolute velocity of the liquid sheet while the velocity U in Eq. (33) is the relative velocity between the liquid and gas.

For a parallel-sided sheet, the half thickness h is not a function of radial position and thus the above formulation can be used directly to determine the maximum growth rate and corresponding wave number for long waves with Ω_s determined from Eq. (32). However, for attenuating sheets the thickness is inversely proportional to the radial distance from the injector nozzle and thus h in Eq. (32) changes with time. As a result, the growth rate must be integrated over time so that the total growth is used to predict the breakup length for long waves. From Eq. (1), it is clear that $\partial\eta/\partial t = \omega\eta$ and hence

$$\ln\left(\frac{\eta}{\eta_0}\right) = \int_0^t \omega \, dt'. \tag{36}$$

It was shown in the previous section that viscosity has a minor effect on wave growth in the long wave regime. As a result, Eq. (26) can be used in Eq. (36) for simplicity. If the substitution $h = J/t$ is made and the integration is performed, it can be shown that Eq. (36) results in the following expression for the breakup length $L = V\tau$ of the sheet:

$$L = V\left[3\ln\left(\frac{\eta_b}{\eta_0}\right)\right]^{2/3} \left(\frac{J\sigma}{Q^2 U^4 \rho_1}\right)^{1/3} \tag{37}$$

which is similar to the breakup length expression given by Clark and Dombrowski (1972). In the above formulation, V and U are once again the absolute sheet velocity and liquid/gas relative velocity, respectively, and J is a constant. In addition, the most unstable wave number

is given by

$$K_s = \frac{\rho_2 U^2}{2\sigma} \tag{38}$$

for long wave growth.

Ligaments are assumed to form from the sheet fragments at the point of breakup (given by either Eq. (35) or (37) and their diameter can be obtained from a mass balance. For the case of short waves it is assumed that the ligaments are formed from tears in the sheet once per wavelength, and the resulting diameter is given by

$$d_L = \sqrt{\frac{16h}{K_s}} \tag{39}$$

where K_s is determined from Eq. (33). On the other hand, for long wave growth it is assumed that the ligaments are formed from tears in the sheet twice per wavelength and the resulting diameter is given by

$$d_L = \sqrt{\frac{8h}{K_s}} \tag{40}$$

where K_s is now given by Eq. (38).

Since the ligaments are oriented transversely to the sheet flow direction, the surrounding gas is assumed to have little effect on their breakup and surface tension is responsible for destabilization. In addition, the effect of liquid viscosity is to move the most unstable waves to longer wavelengths without altering the range of instability, which is given by $kd_L/2<1$ for the Rayleigh (1879) breakup regime. If it is assumed, as in the work of Dombrowski and Johns (1963), that breakup occurs when the amplitude of the unstable waves is equal to the radius of a ligament, one drop will be formed per wavelength. A mass balance then gives

$$d_D^3 = \frac{3\pi d_L^2}{K_L} \tag{41}$$

for the drop size d_D where K_L is determined from

$$K_L d_L = \left[\frac{1}{2} + \frac{3\mu_1}{2(\rho_1 \sigma d_L)^{1/2}}\right]^{-1/2} \tag{42}$$

which is Weber's result for the wave number corresponding to the maximum growth rate for the breakup of a cylindrical, viscous liquid column (Weber, 1931). Substitution of Eq. (42) into Eq. (41) gives

$$d_D = 1.88 d_L (1 + 3Oh)^{1/6} \tag{43}$$

for the drop diameter where $Oh = \mu_1/(\rho_1 \sigma d_L)^{1/2}$ is the Ohnesorge number.

4.2. Computer model

The breakup length and drop size equations presented above have been implemented in the KIVA-3V code to calculate the behavior of pressure-swirl atomizers. The KIVA-3V code was originally developed at Los Alamos National Laboratory to calculate three-dimensional, transient, reactive flows with sprays, and the numerical details are given by Amsden (1997). In the present simulations, a two-dimensional domain is used, due to the assumed axisymmetry of the injector nozzles.

The present breakup length expressions for short and long wave growth (Eqs. (35) and (37)) require that the velocity of the liquid sheet be known. Schmidt et al. (1999) assumed that the injector exit velocity profile is uniform and that the total velocity is related to the injection pressure Δp by

$$V = k_v \sqrt{\frac{2\Delta p}{\rho_1}} \tag{44}$$

where the velocity coefficient k_v is given by

$$k_v = \max\left[0.7, \frac{4\dot{m}}{\pi d_0^2 \rho_1 \cos\theta}\sqrt{\frac{\rho_1}{2\Delta p}}\right] \tag{45}$$

where $\dot{m}$ and θ are the measured mass flow rate and spray angle, respectively, and d_0 is the injector exit diameter. Details of Eqs. (44) and (45) can be found in the work of Schmidt et al. (1999).

Assuming that Δp is known, Eq. (44) can be used to find V and hence the axial component of the sheet velocity u via:

$$u = V\cos\theta. \tag{46}$$

The initial sheet thickness h_0 is related to $\dot{m}$ and u by conservation of mass:

$$\dot{m} = \pi\rho_1 u h_0 (d_0 - h_0). \tag{47}$$

The thickness of the sheet as a function of the distance from the orifice is calculated assuming that the sheet velocity is constant in time. It is further assumed that the relative velocity between the sheet and the gas is equal to the absolute velocity of the liquid near the injector (i.e., $U = V$). Thus, Eqs. (44)–(47) provide sufficient information for use in the linear stability analysis presented in Sections 2 and 3.

The present injection conditions produce wave growth in the short wave regime, and thus Eqs. (33) and (35) are used for determining breakup length. The thickness at the point of breakup can be calculated from the breakup length and Eqs. (39), (41) and (42) can then be used to predict drop size. The actual drop size is chosen from a Rosin–Rammler distribution with the size predicted from Eq. (41) as the mean size. At the point of primary breakup, the droplets are tracked using the Lagrangian treatment of Dukowicz (1980) and each droplet is assumed to represent a parcel of physically similar drops (i.e., similar kinematic and

thermodynamic properties). The droplets exchange momentum with the gas through source terms in the gas-phase equations. Droplet collision and coalescence are calculated according to the model of O'Rourke (1981). Turbulent dispersion and distortion are also considered, and secondary droplet breakup is calculated using the Taylor Analogy Breakup (TAB) model (O'Rourke and Amsden, 1987). The gas phase equations are solved using the Arbitrary Lagrangian–Eulerian (ALE) algorithm (Amsden, 1997).

5. Application to pressure-swirl atomizers

The proposed model was validated using experimental data from two high-speed, automotive fuel injectors. In both cases, Stoddard Solvent was the working liquid. The first injector, referred to as Injector A in the present work, is a prototype pressure-swirl injector, which has been studied experimentally by Parrish (1997) and computationally by Han et al. (1997). Injector A is an inwardly-opening injector with an air core as shown in Fig. 9(a) with run conditions given in Table 2. Note that the two cases, referred to as Case 1 and Case 2, are simulated for this injector. Case 2 has a shorter injection duration, and hence a higher injection pressure, compared to Case 1. In this injector, the liquid fuel passes through swirl ports, accelerating tangentially, and enters a swirl chamber. The centrifugal motion of the liquid forms a hollow air core. The area of this swirl chamber reduces to a nozzle, further increasing the tangential velocity. The liquid passes through the nozzle and then forms a free sheet which is modeled with Eqs. (44)–(47) in the present work. In addition, Injector A produces a pre-spray during the initial transients. This feature is not related to sheet atomization and was arbitrarily added to the computation by initializing its drop size to the diameter of the injector orifice.

The results of the calculations are compared with photographs taken by Parrish (1997) in Fig. 10. The images were obtained with a CID camera system. The photographs indicate the overall, qualitative agreement between the predictions and the measured spray which is an important check of the droplet–gas interaction models, such as drag and breakup. Both the

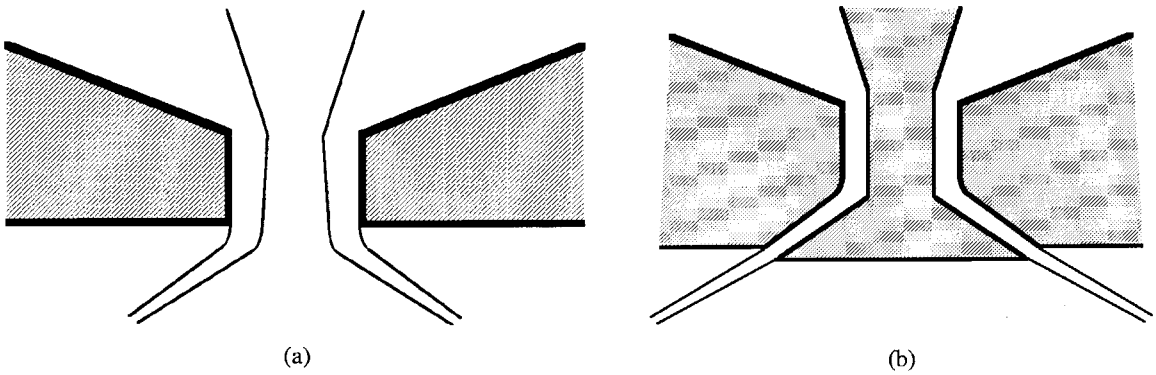

Fig. 9. Schematic of an (a) inwardly-opening and (b) outwardly-opening pressure-swirl atomizer.

Table 2
Injector and liquid characteristics for Injector A

Injection pressure (MPa)	4.86 (Case 1), 6.12 (Case 2)
Mass injected (mg)	44.0
Injection duration (ms)	3.86 (Case 1), 3.4 (Case 2)
Fuel density (g/cm^3)	0.77
Fuel viscosity (g/cm s^{-1})	4.7e−3
Surface tension (g/s^2)	18.16
Ambient pressure (MPa)	0.1
Ambient density (g/cm^3)	1.17e−3

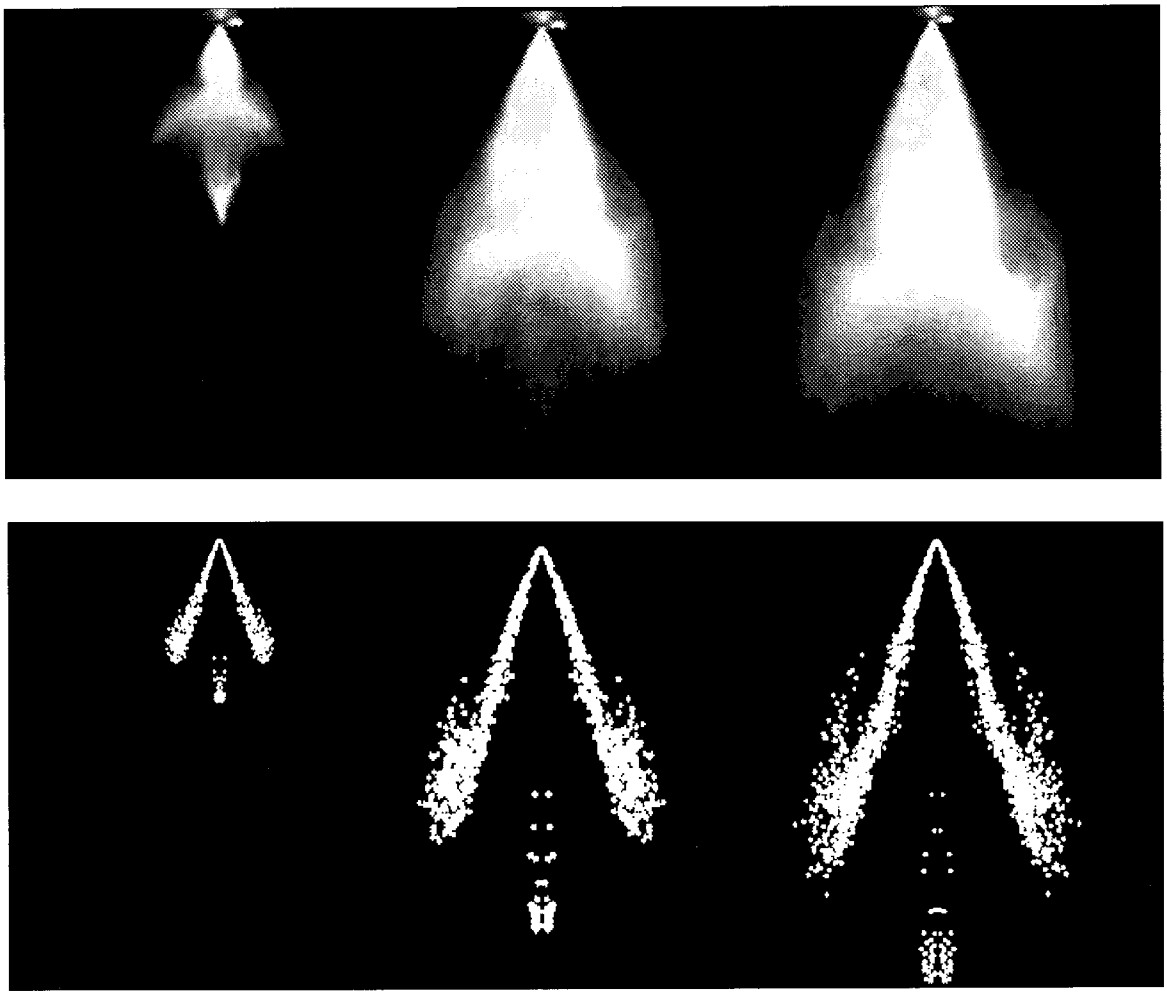

Fig. 10. Comparison of photographs and computer model predictions for Injector A. The numerical results present a two-dimensional slice through the spray, in order to show the spray structure.

photographs and the predictions show the development of an exterior vortex ring that entrains droplets upwards and away from the main spray.

The spray penetration for both the measurements and the computations for Case 1 is shown in Fig. 11 as a function of time. The measured and computed spray penetration were obtained from spray images, examples of which are shown in Fig. 10. The pre-spray and main spray are considered separately, since the main spray is of primary interest in the current study. An accurate prediction of penetration depends on both the droplet size predictions and the droplet velocities. The penetration in Fig. 11 shows excellent agreement; however, this is not a complete validation of the model, since errors in drop size could offset errors in velocity. As a separate check of the model predictions, the predicted drop size was compared to the experimental measurements. The drop size shown in Fig. 12 is the average over a plane located 39 mm downstream of the injector and oriented perpendicular to the spray axis. Experimental drop size distributions were obtained with a diffraction based particle sizing technique and were integrated to calculate the Sauter mean diameter. As described by Han et al. (1997), the line-of-sight particle sizing measurements utilized a CID camera as the detector and a Chin–Shifrin analytical inversion (Chin et al., 1955). Both the experimental and the predicted drop size are initially large due to the pre-spray; however, they both approach a nearly constant value later in the injection. The slight disagreement at the very end of injection suggests that the end of the injection comes too early in the model. Additional comparisons of penetration and Sauter mean diameter for Injector A, Case 2 are presented in Figs. 13 and 14, respectively. As for Case 1, the model predictions agree well with the experimental measurements.

To further validate the model, an outwardly opening injector (called here Injector B) was modeled which includes a pintle and no air core. Injector B was experimentally characterized

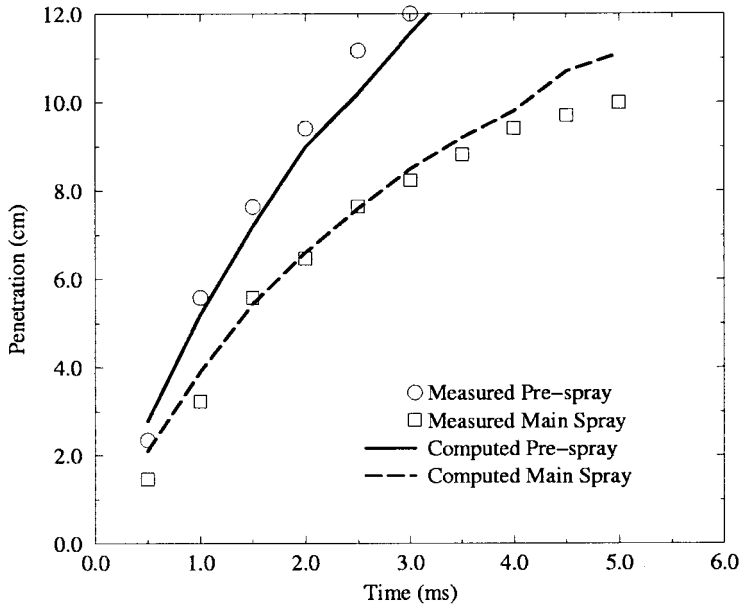

Fig. 11. Measured and predicted spray penetration for Injector A, Case 1.

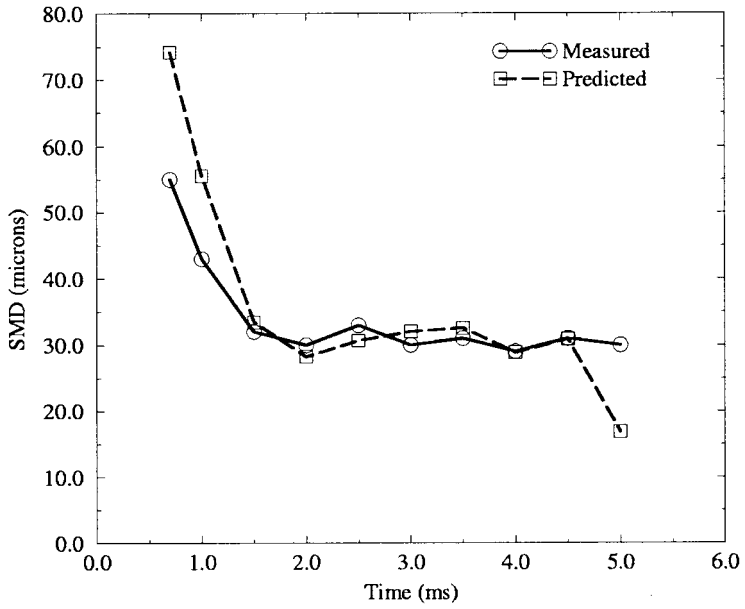

Fig. 12. Measured and predicted Sauter mean diameter for Injector A, Case 1. The drop sizes are averaged over a plane 39 mm downstream of the injector.

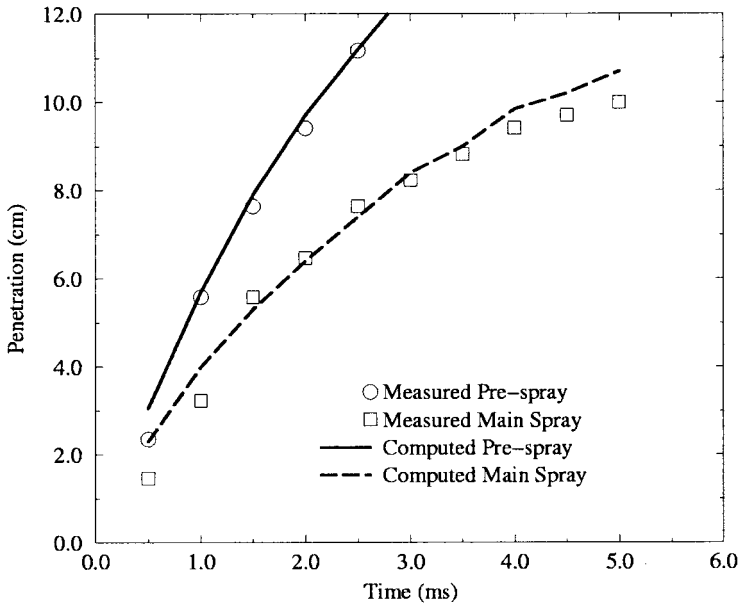

Fig. 13. Measured and predicted spray penetration for Injector A, Case 2.

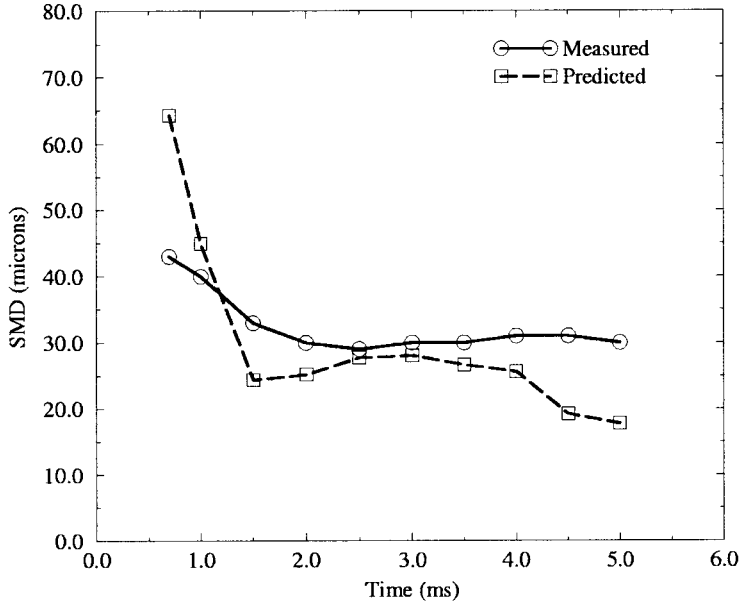

Fig. 14. Measured and predicted Sauter mean diameter for Injector A, Case 2. The drop sizes are averaged over a plane 39 mm downstream of the injector.

by Xu and Markle (1998) and its characteristics are described in Table 3. This injector does not produce a pre-spray due to the pintle. In addition, since the initial thickness of the sheet is determined by the size of the annular gap, one less equation is needed to initialize the calculation. Eq. (44) is not used since the velocity can be calculated from conservation of mass, assuming slug flow at the exit of the injector.

The results for the outwardly opening injector were compared to the published results of Xu and Markle (1998) for room temperature conditions and ambient pressures of 0.1 and 1.5 MPa. The computed spray penetration for the two cases is shown in Fig. 15 alongwith the experimental results. For the atmospheric pressure case, the initial drop diameter was predicted to be 30.9 μm, the breakup length was found to be 1.2 mm and the gas Weber number was

Table 3
Injector and liquid characteristics for Injector B

Injection pressure (MPa)	10.0	10.0
Mass injected (mg)	14.0	14.0
Injection duration (ms)	12.0	13.0
Fuel density (g/cm^3)	0.76	0.76
Fuel viscosity (g/cm s^{-1})	4.25e−3	4.25e−3
Surface tension (g/s^2)	18.16	18.16
Ambient pressure (MPa)	0.1	1.5
Ambient density (g/cm^3)	1.17e−3	1.75e−2

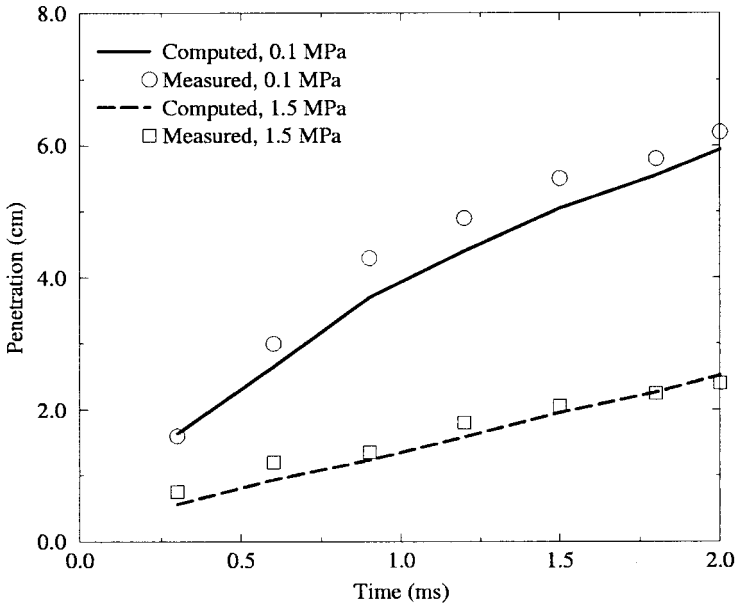

Fig. 15. Measured and predicted penetration for Injector B.

9.76. Secondary drop breakup was found to be important in this case, producing an SMD of 21.7 μm located 30 mm downstream of the injector. For the atmospheric pressure case, Xu and Markle report a somewhat smaller radially-averaged SMD measurement of 15.0 μm at the same axial location.

The effect of increased ambient pressure and density is very significant. The spray tip penetration in a high pressure environment is much less than in an atmospheric pressure case. Both the computed and measured results show a relatively small penetration, as shown in Fig. 15 and thus the numerical model appears to correctly respond to increased ambient pressure and density. The initial drop diameter in this case was predicted to be 10.6 μm. The breakup length was also very small, 37 μm, and the gas Weber number in this case was 121.87. The short breakup length and small droplets are due to the high growth rate. Eq. (33) indicates that high density ratios create faster wave growth. No experimental drop size measurements were made by Xu and Markle for the high ambient pressure case, so the drop size predictions cannot be validated. However, the penetration is consistent with the experimental data.

It is important to note that the present comparisons with experimental measurements validate the spray model as a whole (i.e., the effects of primary atomization, secondary drop breakup, drop drag and collision and coalescence), and do not directly validate the primary breakup expressions presented in this work. However, there are currently no experimental observations of the primary atomization process available for high-speed liquid sheets due to the dense spray and extremely small breakup lengths. As a result, a multi-dimensional code which includes models for all of the key physical processes has been appropriately used for validation purposes in the present work.

6. Conclusions

The atomization of a thin, viscous, liquid sheet in a gas has been studied using a linearized stability analysis. The dispersion relationship has been derived and analyzed. It was found that there are at least two distinct regimes of film atomization. At low gas Weber numbers, the film is broken up by long waves. In this regime, analogous to the first wind induced regime for cylindrical jets, viscosity is unimportant. For gas Weber numbers above 27/16, short waves dominate the breakup process. In this regime, analogous to the second wind induced regime for cylindrical jets, the effect of viscosity is very significant. Using these observations, the dispersion relationship for the two breakup regimes has been simplified.

The simplified dispersion relationships have been implemented into a multi-dimensional CFD code and compared to experimental measurements of spray penetration and drop sizes for two different types of pressure-swirl injectors. The agreement between the predicted and experimental results were very good for both the cases. The numerical predictions of drop size and spray penetration were quantitatively validated. In addition, the predicted spray shape was qualitatively validated by comparison to high-speed photography. Furthermore, the model was found to accurately predict penetration in high-pressure environments.

Acknowledgements

This material is based on the work supported by Renault S.A. and the U.S. Army Research Office under Grant DAAHLO3-92-0122. The authors would like to thank Min Xu of Delphi Automotive Systems and Donald Stanton of Cummins Engine Company for helpful comments.

References

Amsden, A.A., 1997. KIVA–3V: a block-structured KIVA program for engines with vertical or canted valves. LA-13313-MS.

Chin, J.H., Sliepcevich, C.M., Tribus, M., 1955. Particle size distribution from angular variation of intensity of forward-scattered light at very small angles. J. Phys. Chem. 59, 841.

Clark, C.J., Dombrowski, N., 1972. Aerodynamic instability and disintegration of inviscid liquid sheets. Proc. Roy. Soc. A 329, 467–478.

Crapper, G.D., Dombrowski, N., Jepson, W.P., Pyott, G.A.D., 1973. A note on the growth of Kelvin–Helmholtz waves on thin liquid sheets. J. Fluid Mech. 57, 671–672.

Dombrowski, N., Hooper, P.C., 1962. The effect of ambient density on drop formation in sprays. Chem. Eng. Sci. 17, 291–305.

Dombrowski, N., Johns, W.R., 1963. The aerodynamic instability and disintegration of viscous liquid sheets. Chem. Eng. Sci. 18, 203–214.

Dukowicz, J.K., 1980. A particle-fluid numerical model for liquid sprays. J. Comput. Phys. 35, 229–253.

Hagerty, W.W., Shea, J.F., 1955. A study of the stability of plane fluid sheets. J. Appl. Mech. 22, 509–514.

Han, Z., Parrish, S., Farrell, P.V., Reitz, R.D., 1997. Modeling atomization processes of pressure-swirl hollow-cone fuel sprays. Atom. Sprays 7, 663–684.

Levich, V.G., 1962. Physicochemical Hydrodynamics. Prentice-Hall, New Jersey.

Li, X., Tankin, R.S., 1991. On the temporal instability of a two-dimensional viscous liquid sheet. J. Fluid Mech. 226, 425–443.

Lin, S.P., Lian, Z.W., Creighton, B.J., 1990. Absolute and convective instability of a liquid sheet. J. Fluid Mech. 220, 673–689.

Mitra, S.K., Li, X., 1998. An integrated predictive model for droplet size distributions. ILASS-Americas, pp. 371–375.

O'Rourke, P.J., 1981. Collective drop effects on vaporizing liquid sprays. Ph.D. Thesis, Princeton University.

O'Rourke, P.J., Amsden, A.A., 1987. The TAB method for numerical calculation of spray droplet breakup. SAE Paper 872089.

Parrish, S.E., 1997. Spray characterization in a motored direct-injection spark-ignited engine. Ph.D. Thesis, University of Wisconsin–Madison.

Rangel, R.H., Sirignano, W.A., 1991. The linear and nonlinear shear instability of a fluid sheet. Phys. Fluids A 3, 2392–2400.

Rayleigh, L., 1879. On the instability of jets. Proc. Lond. Math. Soc. 10, 4–13.

Reitz, R.D., Bracco, F.V., 1986. Mechanisms of breakup of round liquid jets. In: Encyclopedia of Fluid Mechanics. Gulf Pub, Houston, TX, pp. 233–249.

Ren, W.M., Nally, J.F., 1998. Computations of hollow-cone sprays from a pressure-swirl injector. SAE Paper 982610.

Schmidt, D.P., Nouar, I., Senecal, P.K., Hoffman, J., Rutland, C.J., Martin, J., Reitz, R.D., 1999. Pressure-swirl atomization in the near field. SAE Paper 1999-01-0496.

Squire, H.B., 1953. Investigation of the instability of a moving liquid film. Brit. J. Appl. Phys. 4, 167–169.

Stapper, B.E., Sowa, W.A., Samuelson, G.S., 1992. An experimental study of the effects of liquid properties on the breakup of a two-dimensional liquid sheet. ASME Journal of Engineering for Gas Turbines and Power 114, 39–45.

Sterling, A.M., Sleicher, C.A., 1975. The instability of capillary jets. J. Fluid Mech. 68, 477–495.

Taylor, G.I., 1940. Generation of ripples by wind blowing over a viscous fluid. Collected Works of G.I. Taylor 3, 244–254.

VanDerWege, B.A., 1999. The effects of fuel volatility and operating conditions on sprays from pressure-swirl fuel injectors. Ph.D. Thesis, Massachussets Institute of Technology.

Weber, C., 1931. On the breakdown of a fluid jet. Z.A.M.P 11, 136–159.

Weihs, D., 1978. Stability of thin, radially moving liquid sheets. J. Fluid Mech. 87, 289–298.

Xu, M., Markle, L.E., 1998. CFD-aided development of spray for an outwardly opening direct injection gasoline injector. SAE Paper 980493.